Damage-induced basal epithelial cell migration modulates the spatial organization of redox signaling and sensory neuron regeneration

Alexandra M. Fister[1, 2, §], Adam Horn[1, §], Michael Lasarev[3], and Anna Huttenlocher[1, 4, *]

[1]Department of Medical Microbiology and Immunology, University of Wisconsin-Madison, Madison, United States.

[2]Cellular and Molecular Biology Graduate Program, University of Wisconsin-Madison, Madison, United States.

[3]Department of Biostatistics and Medical Informatics, University of Wisconsin-Madison, Madison, United States.

[4]Department of Pediatrics, University of Wisconsin-Madison, Madison, United States.

[§]These authors contributed equally.

[*]Corresponding Author: huttenlocher@wisc.edu

Summary

Epithelial damage leads to early reactive oxygen species (ROS) signaling, which regulates sensory neuron regeneration and tissue repair. How the initial type of tissue injury influences early damage signaling and regenerative growth of sensory axons remains unclear. Previously we reported that thermal injury triggers distinct early tissue responses in larval zebrafish. Here, we found that thermal but not mechanical injury impairs sensory axon regeneration and function. Real-time imaging revealed an immediate tissue response to thermal injury characterized by the rapid Arp2/3-dependent migration of keratinocytes, which was associated with tissue-scale ROS production and sustained sensory axon damage. Isotonic treatment was sufficient to limit keratinocyte movement, spatially restrict ROS production and rescue sensory neuron function. These results suggest that early keratinocyte dynamics regulate the spatial and temporal pattern of long-term signaling in the wound microenvironment during tissue repair.

Introduction

Restoration of tissue function following epithelial injury requires the regeneration and activity of peripheral sensory neurons, which innervate the skin (Mullen et al., 1996; Rabiller et al., 2021; Simões et al., 2014). In response to tissue damage, axonal regeneration requires the clearance of axon fragments by phagocytes followed by new axonal growth (Rasmussen et al., 2015). While peripheral sensory neurons maintain a cell-intrinsic ability to regenerate following injury (Liu et al., 2011; Mahar and Cavalli, 2018; Renthal et al., 2020), local environmental cues also regulate the response of sensory neurons to tissue damage *in vivo*. Recent advances have identified the contribution of supporting cell populations, paracrine biochemical signaling, and biophysical interactions in regulating peripheral sensory axon regeneration (Avraham et al., 2021; Cheah et al., 2017; Villegas et al., 2012). Despite these advances, we have limited understanding of how early collective signaling in the wound microenvironment is organized and leads to sensory axon regeneration and tissue repair.

Keratinocytes are a primary constituent of epithelial tissue and play a critical role in wound healing. In addition to mediating wound closure by actively migrating toward the site of injury, keratinocytes also generate pro-reparative signals such as reactive oxygen species (ROS), which coordinate longer-term repair pathways (Dunnill et al., 2015; Linley et al., 2012; Love et al., 2013; Mittal et al., 2014; Montserrat et al., 2018; Sies and Jones, 2020). While transient and localized ROS production promote regeneration and sensory axon regrowth, chronically elevated ROS are associated with neurodegeneration and disease (Cobb and Cole, 2015; Rieger and Sagasti, 2011). Thus, precise temporal and spatial organization of tissue redox signaling is likely critical for efficient sensory neuron regeneration and tissue repair.

While epithelial tissue is well adapted to repair from mechanical damage, burn wounds heal poorly. Thermal injury results in chronic pain and lack of sensation in the affected tissue, suggesting that an abnormal sensory neuron response contributes to burn wound pathophysiology (Blais et al., 2013; Choinière et al., 1991; Pavoni et al., 2010; Tirado-Esteban et al., 2020; Tsolakidis et al., 2022). Despite this, we lack an understanding of why sensory neuron function is impaired after burn.

Our previous work has demonstrated persistent inflammation and a loss of an organized collagen matrix that impairs healing after thermal injury in larval zebrafish (LeBert et al., 2018, 2015; Miskolci et al., 2019). These features recapitulate human burns and provide an *in vivo* model system to study the regeneration of sensory neurons in the wound microenvironment.

Using real time imaging, we took advantage of the optical transparency of larval zebrafish to dissect dynamic cell-cell interactions in the wound microenvironment following injury. We found that localized thermal injury induced axonal damage in the tail fin. Live imaging revealed that sensory axons are physically displaced and experience damage associated with the rapid collective migration of basal keratinocytes following burn. This early keratinocyte migration also contributes to elevated ROS at the tissue scale. Keratinocyte migration was dependent on Arp2/3 signaling and treatment with the Arp2/3 inhibitor CK666 dampened early wound-localized ROS production after burn, suggesting that dysregulated migration perturbs the temporal and spatial organization of ROS after tissue damage. Inhibiting keratinocyte migration via osmotic manipulation with isotonic solution spatially restricted ROS production and rescued sensory axon regrowth and function. Collectively, our results support the importance of regulated keratinocyte behavior for early temporal and spatial signal control that leads to sensory axon regeneration and tissue repair.

Results

Burn injury induces peripheral sensory axon damage

To visualize sensory neurons responding to tissue injury, we used 3 days post-fertilization (dpf) *Tg(Ngn1:GFP-Caax)* larval zebrafish that express GFP in sensory neurons (Andermann et al., 2002; Blader et al., 2003; McGraw et al., 2008). Larvae were either mechanically injured by tailfin transection or burn as previously described (Figure 1A) (Miskolci et al., 2019). Intravital imaging of larvae beginning at 24 hours post wound (hpw) revealed an abnormal axon morphology in burned larvae compared to mechanical transection, with axons showing fewer branch points (Figure 1B). To evaluate sensory axons following injury, we assessed axon density in the wounded tissue posterior to the notochord 24 hpw. Larval zebrafish caudal fins can regenerate fully by 3 days post-transection,

with 60% of fin regrowth occurring by day 1.5 (Lisse et al., 2015). Following transection, axon density was 89.5 ± 0.02% of the density observed in age-matched uninjured larvae 24 hpw. In contrast, we found that burned larvae had significantly reduced sensory axon density, with an axon density of 63.7 ± 0.02% compared to uninjured fins (Figure 1C). This relative decrease was sustained even 96 hours post wound (hpw) with an axon density of only 65.1 ± 0.04% compared to control (Figure 1C). To test whether this regenerative defect was associated with a defect in sensory neuron function, we assessed the touch responsiveness of wounded tissue. Light pressure was applied by an eyelash brush directly to the wound area, and sensory neuron function was scored by the presence of a tail flick reflex (Granato et al., 1996). As expected, larvae wounded by transection had a nearly 100% response rate 24 hpw, indicating the rapid recovery of sensory neurons following mechanical injury (Figure 1D). In contrast, none of the burned larvae were sensitive to touch 24 hpw with resolution occurring by 96 hpw (Figure 1D). Importantly, all tested larvae exhibited a tail flick reflex when pressure was applied to the trunk, showing that the impaired sensation was limited to the damaged tissue.

We next sought to further investigate sensory neuron function in burned tissue. For this, we assessed wound-induced axonal damage using *Tg(Elavl3:GCaMP5)* zebrafish larvae that express the calcium probe GCaMP under the pan-neuronal Elavl3 promoter. Using these larvae, we observed no noticeable change in GCaMP intensity under homeostatic conditions (Figure 1–figure supplement 1A). While transient calcium increase following cell damage is required for immediate membrane repair and subsequent regeneration, chronically elevated cytosolic calcium is associated with cell degeneration and death (Khaitin, 2021). GCaMP has previously been used as a marker of real-time axonal damage in zebrafish (Adalbert et al., 2012; Linsley et al., 2021; Ziv and Spira, 1993). Therefore, GCaMP can be used for real-time labeling of axon damage in larval zebrafish (Adalbert et al., 2012; Linsley et al., 2021; Ziv and Spira, 1993). Axon damage is characterized by the fragmenting of axons and the formation of small punctae, which are later cleared by phagocytes (Reyes et al., 2004; Villegas et al., 2012). Accordingly, the neurotoxin sodium azide elicited widespread and long-lasting calcium-positive punctae, indicating sustained axonal damage (Figure 1–figure supplement

1A) (Linsley et al., 2021). Unlike Ngn1, the Elavl3 promoter is expressed by both sensory and motor neurons. To ensure that the calcium increase in wounded tissue was specific to sensory axons, sensory neurons were depleted by injecting a morpholino targeting Ngn1 (Cornell and Eisen, 2002). These larvae did not have any obvious developmental defects but lacked responsiveness to touch stimulation, as previously reported (Cornell and Eisen, 2002). As expected, no calcium increase was detected in Ngn1 depleted larvae following injury (Figure 1–figure supplement 1B).

Time-lapse images were taken of Elavl3:GCaMP5 larvae to visually capture instances of axon damage indicated by calcium-positive punctae during the 30 minutes after injury (Figure 1–figure supplement 1C). These images were compared to time-lapse images of sensory neuron-labeled larvae (Figure 1–figure supplement 1D). In agreement with previous observations of axonal damage following mechanical injury (Arrázola et al., 2019; Rasmussen et al., 2015; Rieger and Sagasti, 2011), tailfin transection resulted in spatially localized axonal damage that was almost completely resolved by 1 hpw (Figure 1E). In contrast, burn injury resulted in a distinct temporal and spatial profile of sensory axon damage. While initial wound-induced sensory neuron-specific calcium increase appeared to be localized to burned tissue, axonal damage continued to increase and spread across the tissue for approximately 6 hours (Figure 1E, F). This raised the question of whether axonal damage was restricted to epithelial tissue directly impacted by injury, as observed in transected larvae. To label wounded epithelium, we used the lipophilic dye FM 1-43, which is commonly used to label damaged cell membranes after wounding (Defour et al., 2014; Lauritzen Sønder et al., 2022; McDade et al., 2021; Shannon et al., 2017). Immediately following either transection or thermal injury, axonal damage overlapped spatially with wounded epithelial tissue (Figure 1G, H). However, by 6 hours following burn injury, there was widespread damage to axons that extended beyond the initial wound area (Figure 1G, H). These findings suggest that burn injury induces axonal damage that accumulates over time and is spatially uncoupled from the surrounding epithelial damage.

The burn wound microenvironment contributes to defective axon regeneration and function

To determine if early wound signaling regulates sensory axon regeneration, we used a two-wound model (Figure 2A) to excise the burned tissue at different times post wound. In this system, zebrafish were first injured by either a primary tailfin transection or burn, and then a secondary transection injury was carried out either early at 5 minutes post-wound (mpw) or late at 6 hpw. The secondary transection was performed so that all the burned tissue was excised (Figure 2A, B). As expected, larvae that underwent only transections at both time points had full sensory function by 24 hpw regardless of the timing of the second transection injury, showing that zebrafish efficiently heal after mechanical damage (Figure 2C-E). In burned larvae, early transection after thermal injury (5 mpw) improved sensory axon regeneration and function to levels similar to transected larvae (Figure 2C-E), suggesting that burn injury does not immediately affect sensory axons differently than mechanical damage. However, when burned tissue was excised after 6 hours, significant defects were noted in both axon density and sensory function compared to larvae that either received two transection injuries or had burned tissue transected at 5 mpw (Figure 2C-E). These findings suggest that the local wound environment modulates sensory axon outcomes following burn injury, and that events in the first 6 hours after injury impact longer term sensory axon repair.

Burn injury induces the early collective movement of keratinocytes and sensory axons

To understand how burn injury damages sensory axons, we performed live imaging of epithelial keratinocytes, which closely associate with sensory axons (O'brien et al., 2012; Rieger and Sagasti, 2011; Rosa et al., 2022). Live-imaging of *Tg(Krt4:UtrCH-GFP)* larvae that express the actin probe Utrophin under a pan-keratinocyte promoter allowed for visualization of keratinocyte dynamics following either mechanical or burn injury. In response to transection, we initially observed characteristic epithelial cell contraction at the wound edge; however, keratinocytes distal to the wound edge remained relatively stationary (Figure 3A; Supplemental Movie 1). In contrast, burn wounding resulted in a rapid collective movement of keratinocytes toward the site of tissue damage (Figure 3–figure supplement 2A). To quantify the rapid movement of keratinocytes in burn injured

larvae, we used *Tg(Krtt1c19e:acGFP)* zebrafish to specifically label motile basal epithelial cells (Lee et al., 2014). Live-imaging experiments revealed that basal keratinocytes, on average, moved a total distance of 205.7±10.7 µm in the first hour following burn injury, which was significantly greater than the 58.9±5.8 µm of migration observed following tailfin transection (Figure 3B; Figure 3–figure supplement 2A). Although keratinocytes moved as a collective in response to burn injury, they exhibited chaotic movement and appeared to be loosely associated with their neighbors.

To determine if this process was due to active migration, time-lapse imaging was performed using *Tg(Krt4:Lifact-mRuby)* larvae to visualize actin dynamics of both the superficial and basal layers. Unwounded larvae had regularly shaped keratinocytes with even actin distribution around the cell periphery in both the superficial and basal layers (Figure 3C), indicative of a non-migratory epithelium. Superficial keratinocytes in burned larvae were elongated and had an even actin distribution, but the basal keratinocytes showed actin localization to the leading edge with the formation of lamellipodia (Figure 3C), suggesting that the superficial keratinocytes are being pulled by the motile basal keratinocytes.

The axons of sensory neurons are ensheathed within actin-rich channels running through basal keratinocytes (O'brien et al., 2012; Shen et al., 2019). Given the chaotic and sustained keratinocyte migration associated with burn injury, we next tested if sensory axons are displaced along with associated migrating keratinocytes. Simultaneous imaging of basal keratinocytes and sensory axons following thermal injury revealed that sensory axon movement is coordinated with keratinocyte migration (Figure 3D; Supplemental Movie 2). To characterize the kinetics of axonal damage following burn, time lapse movies were performed with *Tg(Elavl3:GCaMP5)* larvae to determine if the onset of axonal damage occurs during basal keratinocyte migration. Within the first hour after burn, calcium-positive punctae were identified that coincided with keratinocyte migration, indicating that early keratinocyte migration was associated with the initial axonal damage (Supplemental Movie 3). To determine if damage was limited to axons, we imaged the cell bodies of peripheral sensory neurons. At 3 days post-fertilization, the skin is innervated by Rohon-Beard (RB) and dorsal root ganglia (DRG) neurons with cell bodies that reside within and just outside the spinal cord, respectively. Following burn

injury, we noted that both the RB and DRG cell bodies that innervate the caudal fin were intact and non-motile in comparison to their pre-burn morphology (Figure 3–figure supplement 1E, F). Taken together, these findings indicate that sensory axons are displaced along with the collective movement of basal keratinocytes following burn, and that this early movement is associated with the start of axonal damage.

The Arp 2/3 inhibitor CK666 impairs initial basal keratinocyte migration and modulates early ROS signaling following burn

We next determined if a known regulator of leading-edge actin dynamics and migration, Arp2/3, modulates the movement of basal keratinocytes after burn (Henson et al., 2015). Treatment with the Arp2/3 inhibitor CK666 limited keratinocyte lamellipodia formation and impaired early keratinocyte migration, indicating that the early keratinocyte movement is Arp2/3 dependent (Figure 4A-C). Although early migration was impaired, by 40 mpw the migration was not significantly different between control and CK666 treated larvae, suggesting that CK666 treatment only inhibits early keratinocyte migration. To determine if this early treatment altered signaling in wounded tissue, we probed the effects of CK666 treatment on the generation of reactive oxygen species (ROS) signaling at the burn wounds. It is known that efficient tissue repair after injury relies on coordinated ROS production by epithelial cells (Yoo et al., 2012; Enyedi and Niethammer, 2015; Jelcic et al., 2019). Following mechanical injuries such as tailfin transection or laser ablation, transient and localized H_2O_2 also promotes sensory axon regeneration and wound healing (Diaz et al., 2022; Rieger and Sagasti, 2011). Because of this ROS requirement, we hypothesized that the robust keratinocyte movement and sustained damage in burned tissue may result in dysregulated ROS production. To test this, H_2O_2 level was determined using the fluorescent dye pentafluorobenzenesulfonyl fluorescein (Pfbsf), an established readout of ROS production that has previously been used in larval zebrafish (Maeda et al., 2004; Niethammer et al., 2009). Early after burn wounding, there was robust generation of hydrogen peroxide in burned tissue that was dampened in CK666 treated larvae. In the presence of CK666, H_2O_2 production was concentrated at the wound edge, similar to what has been reported with tail transection (Figure 4D, E).

These findings suggest that early migration alters the temporal and spatial distribution of ROS after wounding. Interestingly, CK666-treated larvae had no significant difference in axon damage or regeneration 24 hours after burn compared to controls, although there was a trend toward improved sensory function (Figure 4F-H). Taken together, the findings suggest that keratinocyte migration regulates early tissue scale ROS production after burn injury.

The direct effects of early ROS signaling on burn wound healing were also tested using the drug Diphenyleneiodonium (DPI) to inhibit ROS production (Li and Trush, 1998; Niethammer et al., 2009 Yoo 2012). Treatment longer than 1 hpw was not possible due to toxicity. With this short treatment, larvae showed some improvement in axon density and touch sensitivity, although it was not statistically significant (Figure 4–figure supplement 2B-D). These data suggest that early ROS inhibition is not sufficient to rescue axon regeneration and function, although it is possible that short term dampening of ROS may improve sensory neuron function.

Isotonic solution limits keratinocyte movement induced by burn injury and alters the temporal and spatial distribution of redox signaling

Previous studies have demonstrated that the presence of an osmotic gradient promotes keratinocyte migration via cell swelling in response to mechanical injury (Gault et al., 2014). To determine if other treatments that affect keratinocyte migration also impact tissue scale ROS production after burn, we determined if altering osmotic balance impacts keratinocyte migration and the distribution of ROS signaling after burn. Under control conditions, zebrafish are maintained in hypotonic solution. Removing this osmotic gradient by wounding larvae in the presence of solution that is isotonic to the interstitial fluid has previously been shown to inhibit keratinocyte migration following mechanical injury and impair wound healing (Gault et al., 2014; Kennard and Theriot, 2020). We found that wounding in the presence of an isotonic solution prevented the rapid movement of keratinocytes in response to a burn. Within the first hour following burn injury, keratinocyte average speed was reduced from 0.059 µm/s in control medium to 0.003 µm/s in isotonic medium (Figure 5A-C; Supplemental Movie 4). Immediately following burn injury, the level of H_2O_2 was the same between the treatment groups,

indicating that cells wounded in the presence of isotonic solution maintain their normal ability to generate ROS (Figure 5F, G) (Enyedi and Niethammer, 2015). Examining ROS production during the first hour post-burn revealed that control larvae had increased ROS throughout the fin tissue compared to isotonic-treated larvae, while both conditions had comparable levels of ROS at the wound (Figure 5D, E). At 6 hours post burn, H_2O_2 production was no longer localized to the wound edge in control burned larvae and had increased throughout the tailfin. By contrast, H_2O_2 remained restricted to the wound edge in larvae burned in the presence of isotonic solution, displaying a similar localized pattern to that observed after mechanical injury (Figure 5F) (Jelcic et al., 2019; Korte et al., 2022). Quantification revealed that H_2O_2 level at the wound edge was similar between control and isotonic treated larvae 6 hpw. However, the level of H_2O_2 was approximately 6-fold lower in the fin epithelial tissue adjacent to the burn wound with isotonic treatment (Figure 5F, H). These findings suggest that robust keratinocyte movement induced by burn injury generates an oxidative environment at the tissue-scale.

Isotonic medium is sufficient to improve sensory neuron regeneration and function after burn

We next assessed sensory axon damage after burning in isotonic solution. Immediately following injury, larvae burned in isotonic solution displayed axon damage similar to larvae injured in control medium (Figure 6A). However, 6 hpw, axonal damage in isotonic treated larvae was reduced and remained restricted to the site of injury, similar to the spatially restricted H_2O_2 signal induced by isotonic treatment (Figure 6B). Accordingly, larvae burned in isotonic medium had significantly greater axon density 24 hpw, and more than 85% of isotonic treated larvae had normal sensory function by 24 hpw (Figure 6C-E). To determine if the benefit of isotonic solution was due to its ionic composition, we tested the effects of an isotonic solution of the sugar D-Sorbitol. We also found that an isotonic solution with D-Sorbitol limited basal keratinocyte migration and had normal axon density and sensory function 24 hpw, suggesting that the benefit of isotonic solution is independent of effects on electrical cues (Figure 6–figure supplement 3A-C).

To determine if early keratinocyte migration contributes to the impact of isotonic solution on sensory neuron function at later time points, we treated with isotonic solution starting 1 hour following

burn injury (Figure 6F). When isotonic medium was added 1 hpw, after keratinocyte migration was complete, there was no rescue of ROS production in either the wound area or the fin 6 hpw (Figure 6 G, H). Additionally, there was no improvement in sensory axon density or function 24 hpw, supporting the idea that early wound events during the first hour are critical for their effects on later sensory neuron function (Figure 6I-K). Collectively, these findings suggest that early keratinocyte movement after burn coordinates spatial redox signaling and impacts sensory axon regeneration.

Discussion

Tissue repair requires the coordination of signaling across spatial and temporal scales. Our prior work has shown that early ROS signaling immediately after mechanical damage is necessary for longer term tissue repair (Yoo et al., 2012). Wound-induced ROS production is also required for leukocyte recruitment, ECM remodeling, and sensory axon regeneration in response to tissue injury (LeBert et al., 2018; Niethammer et al., 2009; Rieger and Sagasti, 2011; Yoo et al., 2011). While the requirement of ROS production following tissue injury is clear, we lack an understanding of how early redox signaling is coordinated temporally and spatially to mediate long-term tissue repair. We recently reported that burn injury induces a distinct repair response with impaired collagen remodeling and delayed healing (LeBert et al., 2018; Miskolci et al., 2019). In light of the known defect in sensory function after burn injuries in humans, we sought to determine how the early epithelial response modulates sensory axon recovery. Our findings suggest that early damage-induced keratinocyte movement plays a role in the spatial patterning of ROS production in the wound microenvironment and impacts the ability of sensory axons to regenerate.

Collective keratinocyte migration is conserved across species and is required to mediate wound closure after tissue injury (Kirfel and Herzog, 2004; Mayor and Etienne-Manneville, 2016). While collective cell migration has been observed in larval zebrafish previously (Olson and Nechiporuk, 2021; Yamaguchi et al., 2022), its contribution to tissue repair remains unclear. In comparison to the organized movement associated with keratinocyte response to mechanical injury, our observations here identify excessive keratinocyte migration as a defining feature of the response to burn injury.

Basal keratinocyte migration following burn injury appeared to lack a stereotypical leader-follower dynamic, with cells instead moving independently of one another but as a collective group. This observation suggests that collective keratinocyte migration is a feature of tissue repair in larval zebrafish regardless of the mode of injury and that its regulation is required for the success of long-term healing. Indeed, we provide evidence that early migration and formation of lamellipodia in basal keratinocytes requires Arp2/3 signaling, and that this aberrant migration regulates the temporal and spatial distribution of early redox signaling in the wound tissue. However, Arp2/3 inhibition did not lead to sustained control of keratinocyte migration and production of ROS eventually increased throughout the tail fin. Accordingly, sensory function was not significantly improved at 24 hours post wound.

To further modulate keratinocyte movement, we took advantage of isotonic treatment that is known to affect keratinocyte migration after wounding by tail fin transection. Cell swelling is thought to induce migration by promoting branched actin polymerization and lamellipodia formation (Bera et al., 2022; Han et al., 2012; Sforna et al., 2022), potentially through the activity of mechanically activated ion channels. Previous groups have shown that osmotic differences trigger both ATP release and lamellipodia formation in basal keratinocytes, which promote keratinocyte migration (Chen et al., 2019; Gault et al., 2014). Our results also show that osmotic modulation affects basal keratinocyte motility in response to burn injury. Interestingly, limiting keratinocyte motility by isotonic treatment is detrimental to tissue repair following mechanical injury (Gault et al., 2014), but isotonic treatment both rescues epithelial morphology and reduces axon damage following thermal injury. This suggests that there is an optimal amount of keratinocyte movement needed for efficient repair and long-term regeneration.

A conceptual challenge in wound repair has been understanding how early wound-induced events are linked to long-term repair (Sonnemann and Bement, 2011). ROS signaling provides a framework to understand this link due to its requirement for both early wound contraction and long-term regeneration. In zebrafish, the reactive oxygen species H_2O_2 is generated along a tissue-scale gradient with the highest levels at the wound edge (Niethammer et al., 2009). While this spatial gradient undoubtedly directs cell function based on the position along the gradient, uncontrolled ROS

production is damaging to tissues. Therefore, a mechanism must exist to control ROS such that it remains relatively localized to the site of damage and is controlled temporally and spatially. In addition to their early role in wound resealing, keratinocyte redox signaling is critical for long-term repair. Cell swelling induces cPLA2-dependent 5-oxoETE production and immune cell recruitment (Enyedi et al., 2013). This suggests the signals that control keratinocyte motility may simultaneously modify long-term keratinocyte signaling.

Our findings suggest that cell migration can modulate tissue scale signaling following injury. Importantly, isotonic treatment blocks keratinocyte movement and restores localized ROS signaling at the wound edge. The dependence on migration was supported both by the effects of Arp2/3 inhibition on early ROS signaling, and by the finding that isotonic treatment started after migration was complete (1 hour after injury) did not rescue tissue scale ROS. This suggests that early keratinocyte migration patterns the tissue scale ROS distribution. Additionally, ROS inhibition with the drug DPI provided only slight benefits to axon regeneration. This could be due to treatment being sustained for only 1 hpw, but migration was also not inhibited which further points to the importance of migration in early wound signaling. The finding that isotonic treatment at the time of injury was sufficient to rescue sensory function but treatment after 1 hour did not rescue axon regeneration further highlights the importance of this early motile response for setting up the longer-term repair after damage.

The benefit of a system in which keratinocyte motility controls downstream signaling is two-fold. First, it enables signaling to be scaled to the size of injury. If more cells migrate due to a larger injury, then production of ROS will likewise increase. Second, this system provides a mechanism to control the spatial localization of signaling. Keratinocyte migration requires transiently detaching from neighboring cells. Thus, the act of migrating induces a physical change in the tissue that demarcates the wound region from healthy tissue. It is known that production of ROS promotes keratinocyte motility, and that adhesion is linked to cellular redox state (Dunnill et al., 2015; Mendieta-Serrano et al., 2019). Given these observations, it seems plausible that ROS production in wounded tissue is linked to the biomechanical state of keratinocytes – with low ROS in static, adhered cells, and high

ROS in loosely adhered or migrating cells. A conceptual framework such as this would explain excessive ROS production in burn wounded tissue. Early keratinocyte dynamics in burned tissue are associated with normal wound edge ROS production. However, lack of a migratory stop signal may result in excessive keratinocyte migration and subsequent epithelial damage associated with keratinocytes detaching from the basal lamina. Therefore, failure to restore epithelial homeostasis due to unabated keratinocyte movement may allow for ROS production to continue over time and spread further away from the wound site. Future studies will be aimed at identifying the molecular link between cell migration and tissue scale signaling during tissue repair.

In summary, we have identified early wound-induced keratinocyte migration as a mechanism that controls spatial patterning of long-term wound signaling. These findings highlight the ability of keratinocytes within the wound microenvironment to integrate early signaling and migratory functions that mediate initial wound closure and subsequently regulate spatial tissue signaling necessary for efficient repair of sensory neuron function. Further, our results not only highlight the utility of larval zebrafish for revealing new insights of the tissue response to injury *in vivo*, but also demonstrate the potential for these findings to inform new treatment strategies for wound healing more broadly.

Materials & Methods

Ethics

This study was carried out in accordance with the recommendations from the Guide for the Care and Use of Laboratory Animals from the National Institutes of Health. All zebrafish protocols in this study were approved by the University of Wisconsin-Madison Research Animals Resource Center (Protocol M005405-R02).

Zebrafish maintenance and handling

Adult zebrafish and embryos were maintained as described previously (Houseright et al., 2021; Miskolci et al., 2019). For all experiments, 3 days post- fertilization (dpf) larvae were anesthetized

in E3 medium containing 0.2 mg/mL Tricaine (ethyl 3- aminobenzoate; Sigma-Aldrich) and maintained at 28.5 °C. All transgenic lines including *Tg(Ngn1:GFP- Caax)*(Blader et al., 2003), *Tg(Krt4:LifeAct-mRuby)* (Lam et al., 2015), *Tg(Krt4:UtrCH-GFP)*, *Tg(Krt4:TdTomato)*, *TgBac(Lamc1:Lamc1- sfGFP)* (Yamaguchi et al., 2022), *Tg(ElavI3:GCaMP5)* (Akerboom et al., 2012), *Tg(Krtt1c19e:LifeAct-mRuby)*, and *Tg(Krtt1c19e:acGFP)* were maintained on the AB background strain. To screen larvae for fluorescence, a Zeiss Zoomscope EMS3/SyCoP3 with a Plan-NeoFluar Z objective was used.

Generation of *Tg(Krtt1c19e:LifeAct-mRuby)* transgenic line

The *Krtt1c19e* promoter (Lee et al., 2014) flanked by Age1 and NotI was isolated and cloned into an expression vector containing Lifeact-mRuby and Tol2 elements for genomic integration. 3 nL of solution made of 50 ng DNA and 25 ng Tol2 transposase mRNA were injected into the yolk of one-cell stage embryos. F_0 larvae were raised to adulthood and crossed to adult AB zebrafish. F_2 larvae were screened for mRuby expression and grown to generate stable lines. *Tg(Ngn1:GFP-Caax)* larvae transiently expressing *Krtt1c19e:Lifeact-m*Ruby were used for simultaneous imaging of axon-keratinocyte interactions, and larvae transiently expressing *Krtt1c19e:Lifeact-mRuby* were used to acquire timelapses of basal keratinocyte migration in the CK666 treatment condition.

Caudal fin transection and burn injury

All injuries were applied to fish anesthetized in 1x Tricaine with E3. Transection of the caudal fin was performed on anesthetized larvae in a 60 mm tissue culture-treated dish containing 1x Tricaine with E3. Larvae were cut perpendicular to the caudal notochord boundary using a surgical blade (Feather No. 10, VWR). Burn injury was performed on anesthetized larvae in a 60 mm tissue culture-treated dish containing 1x Tricaine with E3. A fine tip cautery pen (Geiger Medical Technologies) was used to burn the caudal fin until the wounded region reached halfway to the posterior notochord boundary. After injury, larvae were kept in 60 mm dishes and maintained at 28.5 C until imaged. For two-wound experiments, larvae were either transected or burned as described above. Secondary transection,

after either 5 minutes or 6 hours, was performed as described above.

Drug treatment

For all treatments, larvae were incubated in the indicated drug solution for at least 15-30 minutes. Each drug solution was made containing 1x Tricaine with E3 to keep larvae anesthetized during the experiment. Unless indicated otherwise, larvae were in the presence of treatment for the duration of all experiments. All treatments did not obviously impair larval development or health, and axon density in unwounded larvae was measured for each treatment to ensure there were no deficits in axonal patterning (Figure Supplement 3D,E). To elicit sensory axon damage in the absence of a wound, larvae were treated with 1.5% sodium azide (Fisher Scientific). Isotonic medium was prepared by supplementing 1x Tricaine with E3 with either NaCl (Fisher Scientific) or D-Sorbitol (Sigma-Aldrich) to a final concentration of 135 mM. Isotonic medium does not noticeably impair embryonic development or health of the larvae on the time scale used here (Gault et al., 2014; Jelcic et al., 2019). For experiments using CK666 (Sigma), larvae were incubated in 100 µM Ck666 for one hour before wounding and kept in treatment until 6 hpw. The DPI dosage of 20 µM used in this manuscript was was determined by dosage curve of 1 µM to 200 µM. Larvae were pre-treated for 1 hour and then burned and incubated in treatment for 1 hour - treatments over 20 µM or over 1 hpw were detrimental to larval health and development.

Live and time-lapse imaging

Larvae were imaged using a spinning disc microscope (CSU-X, Yokogawa) with a confocal scanhead on a Zeiss Observer Z.1 inverted microscope, Plan-Apochromat NA 0.8/20X objective, and a Photometrics Evolve EMCCD camera. All images were acquired using ZEN 2.6 software. For time lapse imaging, larvae were mounted in a zWEDGI restraining device (Huemer et al., 2016) with the head covered in 2% low-melting point agarose (Sigma- Aldrich). For single time point imaging, anesthetized larvae were mounted in 2% low-melting point agarose on a 35 mm glass-bottom depression dish (CellVis). In all cases, larvae were imaged in E3 medium supplemented with

Tricaine as described above.

Quantification of axon density and sensory function

Axon density was measured by generating maximum intensity z-projected confocal images of the caudal fin using FIJI (Schneider et al., 2012). For every experiment, the caudal fin area posterior to the notochord was outlined using the Polygon tool and measured to obtain a total surface area ROI. Axons inside the outlined area were manually thresholded so all axons posterior to the notochord were labeled and no saturated pixels were present. Density was measured by dividing the area of detected axons by the area of the ROI. In each case, density values of the experimental sample were normalized to the indicated control - either unwounded or control treated fins. Sensory neuron function was determined using a behavioral touch assay (Granato et al., 1996). 3-day post-fertilization larvae were wounded as described above. At the indicated time post-wound, larvae were briefly anesthetized for mounting into the zWEDGI restraining device, with only the head mounted in 2% low-melting point agarose. Fresh E3 was added, and larvae were allowed to rest for one hour. To assess sensory function, the wounded region of caudal fin was touched with the tip of an eyelash brush (No. 1 Superfine Eyelash, Ted Pella) and the presence or absence of a twitch reflex was recorded.

Quantification of axon damage

Maximum intensity z-projected confocal images of the caudal fin were generated using FIJI. For all experiments, the caudal fin area posterior to the notochord was outlined using the Polygon tool and measured to obtain a total surface area ROI. Axon fragments inside the outlined area were manually thresholded so all fragments posterior to the notochord were labeled and no saturated pixels were present, and an area measurement of these thresholded pixels was taken.

Visualization of sensory axon and tissue damage

To visualize damage to sensory axons, *Tg(ElavI3:GCaMP5)* larvae were used. Identical microscope

settings (20x objective, 10% laser, 100 ms exposure, 2 µm step size) were used for all experiments to acquire images and movies. Representative images are maximum intensity z-projections of the caudal fin generated using FIJI. FM 1-43 dye (Life Technologies) was used to visualize tissue damage following transection and burn injury.

For these experiments, larvae were incubated in 1 mg/ml FM 1-43 for 15 minutes prior to injury and through time at which they were imaged. Larvae were maintained at 28.5 C until imaging at the indicated time post- injury.

Quantification of hydrogen peroxide level

Hydrogen peroxide was quantified using pentafluorobenzenesulfonyl fluorescein (Pfbsf, Santa Cruz) (Maeda et al., 2004). Larvae were incubated in 1 µM Pfbsf for 15 minutes prior to injury and maintained in dye solution for the duration of each experiment. Identical microscope settings (10x objective, 1% laser, 50 ms exposure, 3.7 µm step size) were used for all experiments to acquire images and movies. Pfbsf intensity was calculated by generating sum projections and measuring mean gray value of the fin and wound zone in FIJI. Wound zone Pfbsf quantifications were taken by measuring mean gray value of the area posterior to the notochord. For measurements of the fin, mean gray value of the trunk area 200 µm anterior to the tip of the notochord and excluding pigmented skin within the region was measured. Background signal was subtracted for each measurement.

Cell tracking

Basal keratinocyte tracking following tissue injury was performed using *Tg(Krtt1c19e:acGFP)* larvae. Cell tracking was performed using the Spots module in Imaris version 9.8.2 (Bitplane, Zurich, Switzerland). For each larva, 3 representative cells were identified and manual tracking was performed, with the average of these cells being used to generate a single value for further analysis. To control for drift of the entire fin during imaging, non-moving pigment was manually tracked by Brightfield and track length was subtracted from basal keratinocyte movement. In all cases, larvae

were imaged for 1 hour following injury at an interval of 30 seconds.

Morpholino injection

Ngn1 morpholino with the sequence 5'-ACG ATC TCC ATT GTT GAT AAC CTG G-3' (Cornell and Eisen, 2002) was used to prevent sensory neuron formation in Elavl3-GCaMP5 larvae to confirm damage signals were constrained only to axons. 5 ng of Ngn1 morpholino was injected into the yolk of one- to two-cell stage zebrafish embryos. Larvae were incubated at 28.5 C until used for experiments at 3 days post-fertilization. Before use in experiments, larvae were screened by the sensory function assay described above to ensure that sensory neurons were depleted.

Image processing

Images were processed and analyzed using FIJI and Imaris version 9.8.2 as indicated. Supplemental movies were generated in FIJI and edited using Adobe Premiere Pro (Adobe). In Adobe Premiere Pro, pseudocoloring of individual keratinocytes was done using the Color Effects module with manual tracking.

Statistical analysis

Each experimental condition consists of at least three independent biological replicates, defined as three clutches of larvae spawned on three different days. Cell-tracking experiments were analyzed using non- parametric methods (Wilcoxon rank-sum test). Quantification of axon density was analyzed using linear mixed- effect models in which biological replicate was treated as a random effect and experimental conditions (e.g., wound, time, or chemical treatment) treated as fixed factors. Experiments measuring fluorescence intensity (Pfbsf intensity) were analyzed in the same manner, except the response (fluorescence) was log-transformed prior to analysis. Means computed on the log scale estimate the median response when back transformed to original units. At the same time, differences between means (of log-transformed data) become ratios of medians after back transformation to the original scale (Aitkin M et al., 1989). Experiments involving the proportion of fish

that responded to touch were analyzed using a general linear model that included replicate and experimental condition as fixed effects; standard errors used for estimation and testing were adjusted to correct for heteroscedasticity in the proportions (Long and Ervin, 2000). Graphing was performed using GraphPad Prism 9 (GraphPad Software, Inc, San Diego, CA). Sample size is reported for specific experiments in the Figure legends.

Acknowledgements

We would like to thank Dr. Mary Halloran (University of Wisconsin-Madison) for the gift of the *Tg(Ngn1- GFP-Caax)* fish line, Dr. Jan Huisken (University of Göttingen) for the *Tg(Elavl3-GcaMP5)* fish line, Dr. Alvaro Sagasti (University of California Los Angeles) for the *Tg(Krtt1c19e:acGFP)* fish line, and Dr. Holger Knaut (New York University) for the *TgBac(LamC1:LamC1-sfGFP)* fish line. We would like to thank Taylor Schoen and Veronika Miskolci for their critical reading of the manuscript, and the members of the Huttenlocher lab for their thoughtful input throughout this project. The authors acknowledge K99 GM147303 to Adam Horn and R35 GM118027 to Anna Huttenlocher.

Author Contributions

A. Fister, A. Horn, and A. Huttenlocher designed and planned the experimental approach. A. Fister and A. Horn performed all the experiments. M. Lasarev performed all statistical analysis. A. Fister, A. Horn, and A. Huttenlocher wrote the paper.

Declaration of Interests

The authors declare no competing financial interests.

Figure Legends

Figure 1: Peripheral sensory axons have impaired regeneration after burn injury. (A) Schematic of larval zebrafish injury. Gray dashed line denotes area used to measured axon density to the right of the notochord. (B) Confocal max-projected images of sensory axons in uninjured, transected, and burned *Tg(Ngn1:GFP-Caax)* caudal fins 24 hpw. (C) Quantification of axon density for uninjured, transected, and burned larvae in the wound area 24-96 hpw. N>20 larvae per condition from 4 replicates. (D) Quantification of sensory perception for uninjured, transected, and burned larvae 24-96 hpw. N>32 larvae per condition from 4 replicates. (E) Confocal time series images of axonal damage, indicated by calcium-positive punctae (black dots), in *Tg(Elavl3:GCaMP5)* larvae following either transection or burn injury. Each series follows one representative larva over 6 hpw. (F) Quantification of axon damage area in transected and burned larvae 6 hpw. N>12 larvae per condition from 2 replicates. (G) Images of larvae either transected or burned in the presence of FM 1-43 dye. White dashed box denotes area of uninjured tissue in which axonal damage appears in H. (H) Images show axonal damage following transection or burn injury. Red dashed box corresponds to the tissue region highlighted in G. In all cases, scale bars=20 µm.*p<0.05, **p<0.01, ***p<0.001, ns=not significant.

Figure 2: The burn wound microenvironment contributes to impaired sensory axon regeneration. (A) Schematic of two-wound experiment design. (B) Confocal max-projected images of FM dye staining following secondary transection in the two-wound experiment at 5 mpw and 6 hpw. (C) Images of sensory axons in larvae subjected to an initial transection or burn injury followed by subsequent transection either early (5 mpw) or late (6 hpw). (D) Quantification of axon density in wounded tissue 24 hpw from larvae wounded as in B. N>28 larvae per condition from 3 replicates. (E) Quantification of sensory perception in wounded tissue 24 hpw from larvae wounded as in B. N=24 larvae each from 3 replicates. In all cases, scale bars=20 µm. *p<0.05, ***p<0.001, ns=not significant.

Figure 3: Burn injury induces coordinated keratinocyte and sensory axon movement. (A) Confocal max-projected time-series images of *Tg(Krt4:UtrCH-GFP)* larvae after either transection or burn injury. Yellow pseudocolored cells and colored tracks highlight keratinocyte displacement. Scale bar=20 µm. (B) Quantification of keratinocyte movement distance over 1 hpw. N= 8 larvae each collected from 3 replicates. (C) Confocal max-projected images of superficial and basal keratinocytes in *Tg(Krt4:Lifeact-mRuby)* labeled larvae. Left, superficial keratinocytes. Middle, basal keratinocytes. Right, Merge. Superficial and basal cell images were taken from the same z-stack and pseudocolored to match the appropriate cell layer. Dashed lines outline one individual keratinocyte. Scale bar=10 µm. (D) Confocal max-projected time-series images of sensory axons and basal keratinocytes in dual-labeled *Tg(Krt4:Lifeact-mRuby); Tg(Ngn1:GFP-Caax)* larvae unwounded or after burn. Arrows highlight coincident movement between keratinocytes and associated sensory axons. Unless otherwise stated, scale bar=20 µm. ***p<0.001.

Figure 4: The Arp 2/3 inhibitor impairs early keratinocyte movement and alters the spatial distribution of reactive oxygen species signaling. (A) Confocal max-projected images of control or CK666-treated transiently injected *Tg(Krtt1c19e:Lifeact-mRuby)* larvae. Arrows point to lamellipodia in the control larva, and lack of lamellipodia in the CK666-treated larva. Scale bar=10 µm. (B) Plot of keratinocyte speed over 1 hpw as treated in A. N=10 larvae each collected from 3 replicates. (C) Plot of keratinocyte distance moved over 1 hpw as treated in A . N=10 larvae each collected form 3 replicates. (D) Confocal sum-projected time-series images of hydrogen peroxide level (Pfbsf intensity) in 1 larva over 1 hpw in the indicated treatment. (E) Quantification of Pfbsf intensity in the wound or fin area of the represented larva after burn injury as treated in D over 1 hpw. N=1 representative larva per condition. (F) Confocal max-projected images of sensory axons 24 hpw in larvae wounded in control medium or CK666. (G) Quantification of axon density 24 hpw in larvae treated as in J. N>22 larvae per condition from 4 replicates. (H) Quantification of sensory perception 24 hpw in larvae treated as in J. N=32 larvae per condition from 4 replicates. Unless otherwise specified, scale bars=20 µm. ns=not significant.

Figure 5: Treatment with isotonic solution inhibits keratinocyte migration and dampens ROS signaling. (A) Confocal time-series images of basal keratinocyte movement in *Tg(Krtt1c19e:acGFP)* larvae over 1 hpw after burn injury in the indicated treatment. (B) Plot of basal keratinocyte average speed over 1 hpw treated as in A. N=10 larvae per condition collected from 3 replicates. (C) Distance of keratinocyte movement over 1 hpw treated as in A. N=10 larvae per condition collected from 3 replicates. (D) Confocal sum-projected, heat mapped time-series images of hydrogen peroxide level (Pfbsf intensity) over 1 hpw as treated in A. (E) Quantification of Pfbsf intensity in the wound or fin area of the represented larva after burn injury as treated in D over 1 hpw. N=1 representative larva per condition. (F) Confocal sum-projected images of Pfbsf intensity in the fin and wound zone either 0 or 6 hours following burn injury. Dashed red line denotes the boundary between the wound area and distal fin tissue. Scale bar=50 µm. (G) Quantification of mean Pfbsf fluorescence intensity (MFI) immediately (0 hpw) after burn injury normalized to the control condition. N>27 larvae per condition from 3 replicates. (H) Quantification of mean Pfbsf fluorescence intensity 6 hpw in the indicated region of the fin normalized to the control condition. N>26 larvae per condition from 3 replicates. Unless otherwise indicated, scale bars=20 µM. *$p<0.05$, ***$p<0.001$, ns=not significant.

Figure 6: Isotonic treatment improves axon regeneration. (A) Confocal max-projected images of axon damage in control or isotonic treated *Tg(Elavl3:GCaMP5)* larvae 0 or 6 hpw. (B) Quantification of axon damage in control and isotonic treated burned fins at 6 hpw as treated in A. N=16 larvae per condition from 3 replicates. (C) Confocal max-projected images of sensory axons in larvae 24 hpw as treated in A. (D) Quantification of axon density 24 hpw in larvae treated as depicted in C. N>30 larvae per condition from 3 replicates. (E) Quantification of sensory perception 24 hpw in larvae treated as in C. N=24 larvae each from 3 replicates. (F) Schematic illustrating the different isotonic treatment paradigms that are being compared. (G) Confocal sum-projected images of pfbsf intensity in control and isotonic +1 hpw treated burned larvae. Dashed red line denotes the boundary between the wound area and distal fin tissue. White dashed line denotes the fin. (H) Quantification of mean Pfbsf

fluorescence intensity (MFI) 6 hpw in the indicated region of the fin normalized to the control condition. N=31 larvae per condition from 3 replicates. (I) Confocal max-projected images of sensory axons 24 hpw in burned control or isotonic treated larvae starting 1 hpw. (J) Quantification of axon density 24 hpw in larvae treated as in D. N=29 larvae per condition from 3 replicates. (K) Quantification of sensory perception 24 hpw in larvae treated as in D. N=24 larvae per condition from 3 replicates. Unless otherwise indicated, scale bars=20 µm. *p<0.05, **p<0.01, ns=not significant.

Supplemental Figures

Supplemental Figure 1: Elavl3-GCaMP5 transgenic fish show sensory axon damage. (A) Confocal max-projected images of axon damage in *Tg(Elavl3:GCaMP5)* larval zebrafish caudal fins either untreated or 30 minutes post-treatment with the neurotoxin sodium azide (NaN_3, 1.5% final concentration). Sensory neuron damage is indicated by calcium-positive axon fragments (black dots). Dashed black lines denote the fin edge. Black boxes highlight area of inset, shown below. (B) Confocal max-projected images of *Tg(Elavl3:GCaMP5)* larvae injected with Ngn1 morpholino both before and 5 minutes after the indicated injury. (C) Confocal max-projected images of *Tg(Elavl3:GCaMP5)* larvae taken from a time series. Red dashed box denotes inset area shown on right of a sensory axon fragmenting over a period of 30 minutes. (D) Confocal max-projected images of *Tg(Ngn1:GFP-Caax)* larvae taken from a time series. Red dashed box denotes inset area shown on right of a sensory axon fragmenting over a period of 30 minutes. (E) Schematic of Rohon-Beard (green) and Dorsal Root Ganglia (blue) soma localization in 3 dpf zebrafish. Red box denotes area in which the image shown in F was acquired. (F) Representative confocal max-projected image of intact RB and DRG somas 24 hpw in a *Tg(Ngn1:GFP-Caax); Tg(Krtt1c19e:Lifeact-mRuby)* dual-labeled larva. Arrows denote RB somas, while arrowheads indicate DRG somas. Soma position was unchanged compared to pre-wounding. In all cases, scale bar=20 µm.

Supplemental Figure 2: Inhibition of early ROS signaling does not significantly improve sensory neuron function. (A) Confocal time series of basal keratinocyte, *Tg(Krtt1c19e:acGFP),* movement

after the indicated injury. Yellow pseudocolored cells highlight keratinocyte displacement. (B) Confocal max-projected images of sensory axons treated with DPI. (C) Quantification of axon density 24 hpw in larvae treated as stated in F. N>19 larvae per condition from 3 replicates. (D) Quantification of sensory perception 24 hpw in larvae treated as in F. N=24 larvae each from 3 replicates. Unless otherwise indicated, scale bars=20 µM. ns=not significant.

Supplemental Figure 3: Keratinocyte movement after injury and effect of D-Sorbitol on sensory axon regeneration. (A) Representative max- projected confocal images of sensory axons in control and isotonic D-Sorbitol treated larvae 24 hpw. (B) Quantification of axon density in wounded tissue 24 hpw. N=28 larvae each from 4 replicates. (C) Quantification of sensory perception 24 hpw. N=24 larvae each collected from 4 replicates. (D) Representative max-projected confocal images of sensory axons in unwounded, drug-treated 4 dpf larvae. (E) Quantification of axon density in larvae treated as stated in E. N>15 larvae each from 3 replicates. In all cases, scale bar=20 µm. **p<0.01, ***p<0.001, ns=not significant.

Supplemental Movie Legends

Supplemental Movie 1: Burn injury induces keratinocyte movement. *Tg(Krt4:UtrCH-GFP)* larvae were injured either by tailfin transection (left) or burn (right). While minimal keratinocyte movement is observed following transection, burn injury results in keratinocyte movement toward the wound edge for approximately 1 hour post-wound. Yellow pseudocolored cells indicate representative keratinocyte movement. Images were collected at 2 frames/min. Scale=20 µm.

Supplemental Movie 2: Sensory axons move with associated keratinocytes following injury. Basal keratinocyte (magenta), *Tg(Krtt1c19e:Lifeact-Ruby)*, and sensory axon (cyan), *Tg(Ngn1:GFP-Caax)*, movement was tracked following burn injury. Arrows highlight regions where keratinocyte and sensory axon movement is spatially coincident. Images were collected at 3 frames/min. Scale=10 µm.

Supplemental Movie 3: Tissue movement is associated with axonal damage following burn injury. *Tg(Elavl3:GCaMP5)* larva was burn wounded to track axonal damage, indicated by elevated intracellular calcium (black dots). Damage present at time 0 min is due to the burn wound itself, while new axonal damage coincides with keratinocyte movement. Images collected at 2 frames/min. Scale=20 µm.

Supplemental Movie 4: Wounding in isotonic medium prevents burn-induced keratinocyte movement. Basal keratinocyte, *Tg(Krtt1c19e:acGFP)*, movement was tracked in control (left) and isotonic treated (right) larvae following burn injury. Wounding in the presence of isotonic medium prevents keratinocyte movement associated with burn wounding. Yellow pseudocolored cells indicate representative keratinocyte movement. Images were collected at 2 frames/min. Scale=20 µm.

References

Adalbert R, Morreale G, Paizs ÀM, Conforti L, Walker SA, Roderick HL, Bootman MD, Siklo´s L, Siklo´s S, Coleman MP. 2012. Intra-axonal calcium changes after axotomy in wild-type and slow wallerian degeneration axons. *Neuroscience* **225**:44–54. doi:10.1016/j.neuroscience.2012.08.056

Aitkin M, Anderson D, Francis B, Hinde J. 1989. Statistical Modelling in GLIM. New York: Oxford University Press.

Akerboom J, Chen TW, Wardill TJ, Tian L, Marvin JS, Mutlu S, Calderón NC, Esposti F, Borghuis BG, Sun XR, Gordus A, Orger MB, Portugues R, Engert F, Macklin JJ, Filosa A, Aggarwal A, Kerr RA, Takagi R, Kracun S, Shigetomi E, Khakh BS, Baier H, Lagnado L, Wang SSH, Bargmann CI, Kimmel BE, Jayaraman V, Svoboda K, Kim DS, Schreiter ER, Looger LL. 2012. Optimization of a GCaMP Calcium Indicator for Neural Activity Imaging. *Journal of Neuroscience* **32**:13819–13840. doi:10.1523/JNEUROSCI.2601-12.2012

Andermann P, Ungos J, Raible DW. 2002. Neurogenin1 Defines Zebrafish Cranial Sensory Ganglia Precursors. *Dev Biol* **251**:45–58. doi:10.1006/DBIO.2002.0820

Arrázola MS, Saquel C, Catalán RJ, Barrientos SA, Hernandez DE, Martínez NW, Catenaccio A, Court FA. 2019. Axonal Degeneration Is Mediated by Necroptosis Activation. *Journal of Neuroscience* **39**:3832–3844. doi:10.1523/JNEUROSCI.0881-18.2019

Avraham O, Feng R, Ewan EE, Rustenhoven J, Zhao G, Cavalli V. 2021. Profiling sensory neuron microenvironment after peripheral and central axon injury reveals key pathways for neural repair. *Elife* **10**. doi:10.7554/ELIFE.68457

Bera K, Kiepas A, Godet I, Li Y, Mehta P, Ifemembi B, Paul CD, Sen A, Serra SA, Stoletov K, Tao J, Shatkin G, Lee SJ, Zhang Y, Boen A, Mistriotis P, Gilkes DM, Lewis JD, Fan CM, Feinberg AP, Valverde MA, Sun SX, Konstantopoulos K. 2022. Extracellular fluid viscosity enhances cell migration and cancer dissemination. *Nature 2022 611:7935* **611**:365–373. doi:10.1038/s41586-022-05394-6

Blader P, Plessy C, Strähle U. 2003. Multiple regulatory elements with spatially and temporally distinct activities control neurogenin1 expression in primary neurons of the zebrafish embryo. *Mech Dev* **120**:211–218. doi:10.1016/S0925-4773(02)00413-6

Blais M, Parenteau-bareil R, Cadau S, Ois Berthod F. 2013. Concise Review: Tissue-Engineered Skin and Nerve Regeneration in Burn Treatment. *Stem Cells and Translational Medicine* **2**:545–551. doi:10.5966/sctm.2012-0181

Cheah M, Fawcett JW, Haenzi B. 2017. Differential regenerative ability of sensory and motor neurons. *Neurosci Lett* **652**:35–40. doi:10.1016/J.NEULET.2016.11.004

Chen T, Zhao H, Gao L, Song L, Yang F, Du J. 2019. Hypotonicity promotes epithelial gap closure by lamellipodial protrusion. *Prog Biophys Mol Biol* **148**:60–64. doi:10.1016/J.PBIOMOLBIO.2017.09.021

Choinière M, Melzack R, Papillon J. 1991. Pain and paresthesia in patients with healed burns: An exploratory study. *J Pain Symptom Manage* **6**:437–444. doi:10.1016/0885-3924(91)90043-4

Cobb CA, Cole MP. 2015. Oxidative and Nitrative Stress in Neurodegeneration HHS Public Access. *Neurobiol Dis* **84**:4–21. doi:10.1016/j.nbd.2015.04.020

Cornell RA, Eisen JS. 2002. Delta/Notch signaling promotes formation of zebrafish neural crest by repressing Neurogenin 1 function. *Development* **129**:2639–2648. doi:10.1242/dev.129.11.2639

Defour A, Sreetama SC, Jaiswal JK. 2014. Imaging Cell Membrane Injury and Subcellular Processes Involved in Repair. *J Vis Exp* 51106. doi:10.3791/51106

Diaz AC, Schmidt NA, Yamazaki M, Hsieh CJ, Lisse TS, Rieger S. 2022. Coordinated NADPH oxidase/hydrogen peroxide functions regulate cutaneous sensory axon de- and regeneration. *Proc Natl Acad Sci U S A* **119**:e2115009119. doi:10.1073/PNAS.2115009119/SUPPL_FILE/PNAS.2115009119.SM18.MOV

Dunnill C, Patton T, Brennan J, Barrett J, Dryden M, Cooke J, Leaper D, Georgopoulos NT. 2015. Reactive oxygen species (ROS) and wound healing: the functional role of ROS and emerging ROS-modulating technologies for augmentation of the healing process. *Int Wound J*. doi:10.1111/iwj.12557

Enyedi B, Kala S, Nikolich-Zugich T, Niethammer P. 2013. Tissue damage detection by osmotic surveillance. *Nat Cell Biol* **15**:1123–1130. doi:10.1038/NCB2818

Enyedi B, Niethammer P. 2015. Mechanisms of epithelial wound detection. *Tends in Cell Biology* **25**:398–407. doi:10.1016/j.tcb.2015.02.007

Gault WJ, Enyedi B, Niethammer P. 2014. Osmotic surveillance mediates rapid wound closure through nucleotide release. *Journal of Cell Biology* **207**:767–782. doi:10.1083/jcb.201408049

Granato M, Van Eeden FJM, Schach U, Trowe T, Brand M, Furutani-Seiki M, Haffter P, Hammerschmidt M, Heisenberg CP, Jiang YJ, Kane DA, Kelsh RN, Mullins MC, Odenthal J, Nüsslein-Volhard C. 1996. Genes controlling and mediating locomotion behavior of the zebrafish embryo and larva. *Development* **123**:399–413. doi:10.1242/DEV.123.1.399

Han L, Mao Z, Wu J, Zhang Y, Gao C. 2012. Influences of surface chemistry and swelling of salt-treated polyelectrolyte multilayers on migration of smooth muscle cells. *J R Soc Interface* **9**:3455–3468. doi:10.1098/RSIF.2012.0546

Henson JH, Yeterian M, Weeks RM, Medrano AE, Brown BL, Geist HL, Pais MD, Oldenbourg R, Shuster CB. 2015. Arp2/3 complex inhibition radically alters lamellipodial actin architecture, suspended cell shape, and the cell spreading process. *Mol Biol Cell* **26**:887–900. doi:10.1091/mbc.E14-07-1244

Houseright RA, Miskolci V, Mulvaney O, Bortnov V, Mosher DF, Rindy J, Bennin DA, Huttenlocher A. 2021. Myeloid-derived growth factor regulates neutrophil motility in interstitial tissue damage. *J Cell Biol* **220**. doi:10.1083/JCB.202103054

Huemer K, Squirrell JM, Swader R, Lebert DC, Huttenlocher A, Eliceiri KW. 2016. zWEDGI: Wounding and Entrapment Device for Imaging Live Zebrafish Larvae. *Zebrafish* **14**:42–50. doi:10.1089/zeb.2016.1323

Jelcic M, Enyedi B, Niethammer P. 2019. Quantitative Imaging of Endogenous and Exogenous H2O2 Gradients in Live Zebrafish Larvae. *Methods in Molecular Biology* **1982**:283–299. doi:10.1007/978-1-4939-9424-3_17

Kennard AS, Theriot JA. 2020. Osmolarity-independent electrical cues guide rapid response to injury in zebrafish epidermis. *Elife* **9**:1–27. doi:10.7554/ELIFE.62386

Khaitin A. 2021. Calcium in Neuronal and Glial Response to Axotomy. *Int J Mol Sci* **22**. doi:10.3390/IJMS222413344

Kirfel G, Herzog V. 2004. Migration of epidermal keratinocytes: Mechanisms, regulation, and biological significance. *Protoplasma* **223**:67–78. doi:10.1007/S00709-003-0031-5/METRICS

Korte BG, Giese MA, Ramakrishnan G, Ma S, Bennin D, Rindy J, Dewey CN, Huttenlocher A. 2022. Cell Type-Specific Transcriptome Profiling Reveals a Role for Thioredoxin During Tumor Initiation. *Front Immunol* **13**. doi:10.3389/FIMMU.2022.818893

Lam PY, Mangos S, Green JM, Reiser J, Huttenlocher A. 2015. In Vivo Imaging and Characterization of Actin Microridges. *PLoS One* **10**. doi:10.1371/JOURNAL.PONE.0115639

Lauritzen Sønder S, Laage Ebstrup M, Dias C, Sofie A, Heitmann B, Nylandsted J. 2022. Plasma Membrane Wounding and Repair Assays for Eukaryotic Cells. *Bio Protoc* **12**:4437. doi:10.21769/BioProtoc.4437

LeBert D, Squirrell JM, Freisinger C, Rindy J, Golenberg N, Frecentese G, Gibson A, Eliceiri KW, Huttenlocher A. 2018. Damage-induced reactive oxygen species regulate vimentin and dynamic collagen-based projections to mediate wound repair. *Elife* **7**. doi:10.7554/ELIFE.30703

LeBert DC, Squirrell JM, Rindy J, Broadbridge E, Lui Y, Zakrzewska A, Eliceiri KW, Meijer AH, Huttenlocher A. 2015. Matrix metalloproteinase 9 modulates collagen matrices and wound repair. *Development (Cambridge)* **142**:2136–2146. doi:10.1242/DEV.121160/VIDEO-3

Lee RTH, Asharani P V., Carney TJ. 2014. Basal Keratinocytes Contribute to All Strata of the Adult Zebrafish Epidermis. *PLoS One* **9**:e84858. doi:10.1371/JOURNAL.PONE.0084858

Li Y, Trush MA. 1998. Diphenyleneiodonium, an NAD(P)H oxidase inhibitor, also potently inhibits mitochondrial reactive oxygen species production. *Biochem Biophys Res Commun* **253**:295–299. doi:10.1006/BBRC.1998.9729

Linley JE, Ooi L, Pettinger L, Kirton H, Boyle JP, Peers C, Gamper N. 2012. Reactive oxygen species are second messengers of neurokinin signaling in peripheral sensory neurons. *Proc Natl Acad Sci U S A* **109**. doi:10.1073/PNAS.1201544109/-/DCSUPPLEMENTAL/PNAS.201201544SI.PDF

Linsley JW, Shah K, Castello N, Chan M, Haddad D, Doric Z, Wang S, Leks W, Mancini J, Oza V, Javaherian A, Nakamura K, Kokel D, Finkbeiner S. 2021. Genetically encoded cell-death indicators (GEDI) to detect an early irreversible commitment to neurodegeneration. *Nature Communications 2021 12:1* **12**:1–14. doi:10.1038/s41467-021-25549-9

Lisse TS, Brochu EA, Rieger S. 2015. Capturing Tissue Repair in Zebrafish Larvae with Time-lapse Brightfield Stereomicroscopy. *J Vis Exp* 52654. doi:10.3791/52654

Liu K, Tedeschi A, Park KK, He Z. 2011. Neuronal Intrinsic Mechanisms of Axon Regeneration. *Annu Rev Neurosci* **34**:131–152. doi:10.1146/ANNUREV-NEURO-061010-113723

Long JS, Ervin LH. 2000. Using Heteroscedasticity Consistent Standard Errors in the Linear Regression Model. *Am Stat* **54**:217. doi:10.2307/2685594

Love NR, Chen Y, Ishibashi S, Kritsiligkou P, Lea R, Koh Y, Gallop JL, Dorey K, Amaya E. 2013. Amputation-induced reactive oxygen species (ROS) are required for successful Xenopus tadpole tail regeneration. *Nat Cell Biol* **15**:222. doi:10.1038/NCB2659

Maeda H, Fukuyasu Y, Yoshida S, Fukuda M, Saeki K, Matsuno H, Yamauchi Y, Yoshida K, Hirata K, Miyamoto K. 2004. Fluorescent probes for hydrogen peroxide based on a non-oxidative mechanism. *Angew Chem Int Ed Engl* **43**:2389–2391. doi:10.1002/ANIE.200452381

Mahar M, Cavalli V. 2018. Intrinsic mechanisms of neuronal axon regeneration. *Nat Rev Neurosci* **19**:323–337. doi:10.1038/S41583-018-0001-8

Mayor R, Etienne-Manneville S. 2016. The front and rear of collective cell migration. *Nature Reviews Molecular Cell Biology 2016 17:2* **17**:97–109. doi:10.1038/nrm.2015.14

McDade JR, Naylor MT, Michele DE. 2021. Sarcolemma wounding activates dynamin-dependent endocytosis in striated muscle. *FEBS Journal* **288**:160–174. doi:10.1111/FEBS.15556

McGraw HF, Nechiporuk A, Raible DW. 2008. Zebrafish dorsal root ganglia neural precursor cells adopt a glial fate in the absence of neurogenin1. *J Neurosci* **28**:12558–12569. doi:10.1523/JNEUROSCI.2079-08.2008

Mendieta-Serrano MA, Mendez-Cruz FJ, Antúnez-Mojica M, Schnabel D, Alvarez L, Cárdenas L, Lomelí H, Ruiz-Santiesteban JA, Salas-Vidal E. 2019. NADPH-Oxidase-derived reactive oxygen species are required for cytoskeletal organization, proper localization of E-cadherin and cell motility during zebrafish epiboly. *Free Radic Biol Med* **130**:82–98. doi:10.1016/J.FREERADBIOMED.2018.10.416

Miskolci V, Squirrell J, Rindy J, Vincent W, Sauer JD, Gibson A, Eliceiri KW, Huttenlocher A. 2019. Distinct inflammatory and wound healing responses to complex caudal fin injuries of larval zebrafish. *Elife* **8**. doi:10.7554/ELIFE.45976

Mittal M, Siddiqui MR, Tran K, Reddy SP, Malik AB. 2014. Reactive Oxygen Species in Inflammation and Tissue Injury. *Antioxid Redox Signal* **20**:1126–1167. doi:10.1089/ars.2012.5149

Montserrat M, Romero G, Mccathie G, Jankun P, Henry &, Roehl H. 2018. Damage-induced reactive oxygen species enable zebrafish tail regeneration by repositioning of Hedgehog expressing cells. *Nat Commun*. doi:10.1038/s41467-018-06460-2

Mullen LM, Bryant S V., Torok MA, Blumberg B, Gardiner DM. 1996. Nerve dependency of regeneration: the role of Distal-less and FGF signaling in amphibian limb regeneration. *Development* **122**:3487–3497. doi:10.1242/DEV.122.11.3487

Niethammer P, Grabher C, Look AT, Mitchison TJ. 2009. A tissue-scale gradient of hydrogen peroxide mediates rapid wound detection in zebrafish. *Nature* **459**:996–1000. doi:10.1038/nature08119

O'brien GS, Rieger S, Wang F, Smolen GA, Gonzalez RE, Buchanan J, Sagasti A. 2012. Coordinate Development of Skin Cells and Cutaneous Sensory Axons in Zebrafish. *J Comp Neurol* **520**:816–831. doi:10.1002/cne.22791

Olson HM, Nechiporuk A V. 2021. Lamellipodia-like protrusions and focal adhesions contribute to collective cell migration in zebrafish. *Dev Biol* **469**:125–134. doi:10.1016/J.YDBIO.2020.10.007

Pavoni V, Gianesello L, Paparella L, Buoninsegni LT, Barboni E. 2010. Outcome predictors and quality of life of severe burn patients admitted to intensive care unit. *Scand J Trauma Resusc Emerg Med* **18**:1–8. doi:10.1186/1757-7241-18-24/FIGURES/3

Rabiller L, Labit E, Guissard C, Gilardi S, Guiard BP, Moulédous L, Silva M, Mithieux G, Pénicaud L, Lorsignol A, Casteilla L, Dromard C. 2021. Pain sensing neurons promote tissue regeneration in adult mice. *NPJ Regen Med* **6**. doi:10.1038/s41536-021-00175-7

Rasmussen JP, Sack GS, Martin SM, Sagasti A. 2015. Vertebrate Epidermal Cells Are Broad-Specificity Phagocytes That Clear Sensory Axon Debris. *The Journal of Neuroscience* **35**:559–570. doi:10.1523/JNEUROSCI.3613-14.2015

Renthal W, Tochitsky I, Yang L, Cheng YC, Li E, Kawaguchi R, Geschwind DH, Woolf CJ. 2020. Transcriptional reprogramming of distinct peripheral sensory neuron subtypes after axonal injury. *Neuron* **108**:128. doi:10.1016/J.NEURON.2020.07.026

Reyes R, Haendel M, Grant D, Melancon E, Eisen JS. 2004. Slow Degeneration of Zebrafish Rohon-Beard Neurons during Programmed Cell Death. *Developmental Dynamics* **229**:30–41. doi:10.1002/DVDY.10488

Rieger S, Sagasti A. 2011. Hydrogen Peroxide Promotes Injury-Induced Peripheral Sensory Axon Regeneration in the Zebrafish Skin. *PLoS Biol* **9**:1000621. doi:10.1371/journal.pbio.1000621

Rosa JB, Nassman KY, Sagasti A. 2022. Sensory axons induce epithelial lipid microdomain remodeling and determine the distribution of junctions in the epidermis. *Mol Biol Cell*. doi:10.1091/MBC.E22-09-0396/ASSET/IMAGES/LARGE/MBC-34-AR5-G008.JPEG

Schneider CA, Rasband WS, Eliceiri KW. 2012. NIH Image to ImageJ: 25 years of image analysis, Nature Methods. doi:10.1038/nmeth.2089

Sforna L, Michelucci A, Morena F, Argentati C, Franciolini F, Vassalli M, Martino S, Catacuzzeno L. 2022. Piezo1 controls cell volume and migration by modulating swelling-activated chloride current through Ca2+ influx. *J Cell Physiol* **237**:1857–1870. doi:10.1002/JCP.30656

Shannon EK, Stevens A, Edrington W, Zhao Y, Jayasinghe AK, Page-McCaw A, Shane Hutson M. 2017. Multiple Mechanisms Drive Calcium Signal Dynamics around Laser-Induced Epithelial Wounds. *Biophysical Journ* **113**:1623–1635. doi:10.1016/j.bpj.2017.07.022

Shen K, Jiang N, Rasmussen JP, Clanton JA, Rosenberg MF, Luedke KP, Cronan MR, Parker ED, Kim H-J, Vaughan JC, Sagasti A, Parrish JZ. 2019. A conserved morphogenetic mechanism for epidermal ensheathment of nociceptive sensory neurites. *Elife* **8**. doi:10.7554/eLife.42455.001

Sies H, Jones DP. 2020. Reactive oxygen species (ROS) as pleiotropic physiological signalling agents. *Nature Reviews*. doi:10.1038/s41580-020-0230-3

Simões MG, Bensimon-Brito A, Fonseca M, Farinho A, Valério F, Sousa S, Afonso N, Kumar A, Jacinto A. 2014. Denervation impairs regeneration of amputated zebrafish fins. *BMC Dev Biol* **14**. doi:10.1186/S12861-014-0049-2

Sonnemann KJ, Bement WM. 2011. Wound Repair: Toward Understanding and Integration of Single-Cell and Multicellular Wound Responses. *Annu Rev Cell Dev Biol* **27**:237. doi:10.1146/ANNUREV-CELLBIO-092910-154251

Tirado-Esteban A, Seoane JL, Serracanta Domènech J, Aguilera-Sáez J, Barret JP. 2020. Sensory alteration patterns in burned patients. *Burns* **46**:1729–1736. doi:10.1016/J.BURNS.2019.08.005

Tsolakidis S, Alharbi Z, Rennekampff HO, Schmidhammer MR, Schmidhammer R, Rosenauer R. 2022. “Out of Touch”—Recovering Sensibility after Burn Injury: A Review of the Literature. *European Burn Journal* **3**:370–376. doi:10.3390/EBJ3020032/S1

Villegas R, Martin SM, O KC, Carrillo SA, Sagasti A, Allende ML. 2012. Dynamics of degeneration and regeneration in developing zebrafish peripheral axons reveals a requirement for extrinsic cell types. *Neural Dev* **7**:19. doi:10.1186/1749-8104-7-19

Yamaguchi N, Zhang Z, Schneider T, Wang B, Panozzo D, Knaut H. 2022. Rear traction forces drive adherent tissue migration in vivo. *Nat Cell Biol* **24**:194. doi:10.1038/S41556-022-00844-9

Yoo SK, Freisinger CM, LeBert DC, Huttenlocher A. 2012. Early redox, Src family kinase, and calcium signaling integrate wound responses and tissue regeneration in zebrafish. *J Cell Biol* **199**:225–234. doi:10.1083/jcb.201203154

Yoo SK, Starnes TW, Deng Q, Huttenlocher A. 2011. Lyn is a redox sensor that mediates leukocyte wound attraction in vivo. *Nature* **480**:109. doi:10.1038/NATURE10632

Ziv NE, Spira ME. 1993. Spatiotemporal Distribution of Ca2+ Following Axotomy and Throughout the Recovery Process of Cultured Aplysia Neurons. *European Journal of Neuroscience* **5**:657–668. doi:10.1111/J.1460-9568.1993.TB00531.X

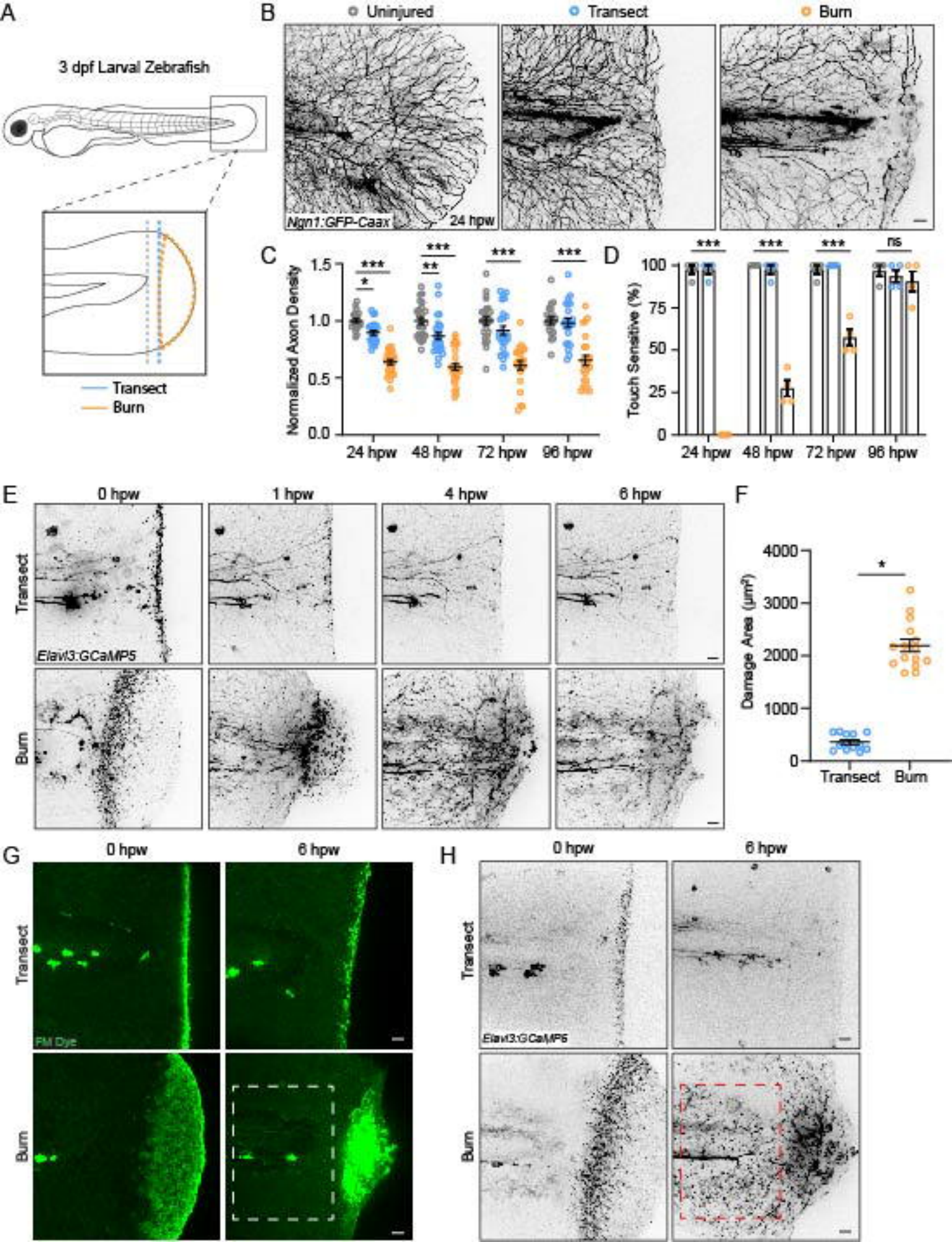
A
3 dpf Larval Zebrafish
Transect
Burn
B
Uninjured
Transect
Burn
Ngn1:GFP-Caax
24 hpw
C
Normalized Axon Density
1.5
1.0
0.5
0.0
***
*
***
**
***
***
24 hpw
48 hpw
72 hpw
96 hpw
D
Touch Sensitive (%)
100
75
50
25
0
***
***
***
ns
24 hpw
48 hpw
72 hpw
96 hpw
E
0 hpw
1 hpw
4 hpw
6 hpw
Transect
Burn
Elavl3:GCaMP5
F
Damage Area (μm²)
4000
3000
2000
1000
0
*
Transect
Burn
G
0 hpw
6 hpw
Transect
Burn
FM Dye
H
0 hpw
6 hpw
Transect
Burn
Elavl3:GCaMP5

A

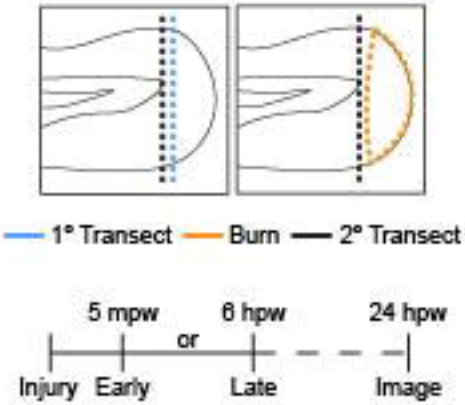
1° Transect
Burn
2° Transect
5 mpw
or
6 hpw
24 hpw
Injury
Early
Late
Image

B

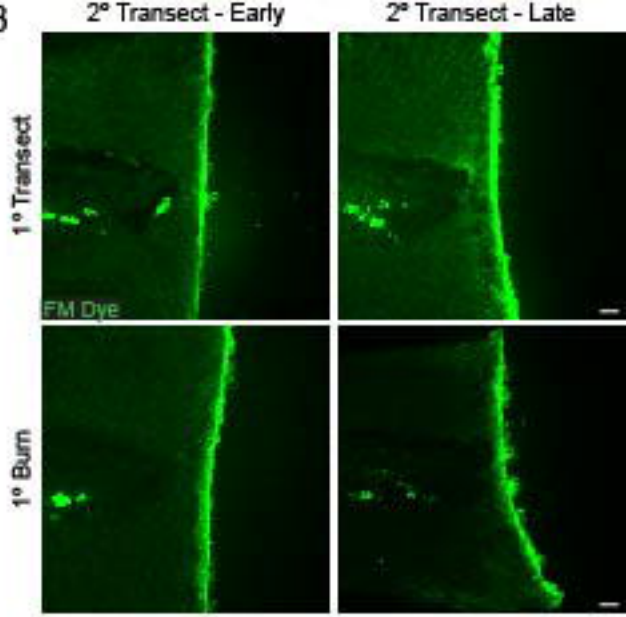
2° Transect - Early
2° Transect - Late
1° Transect
1° Burn
FM Dye

C

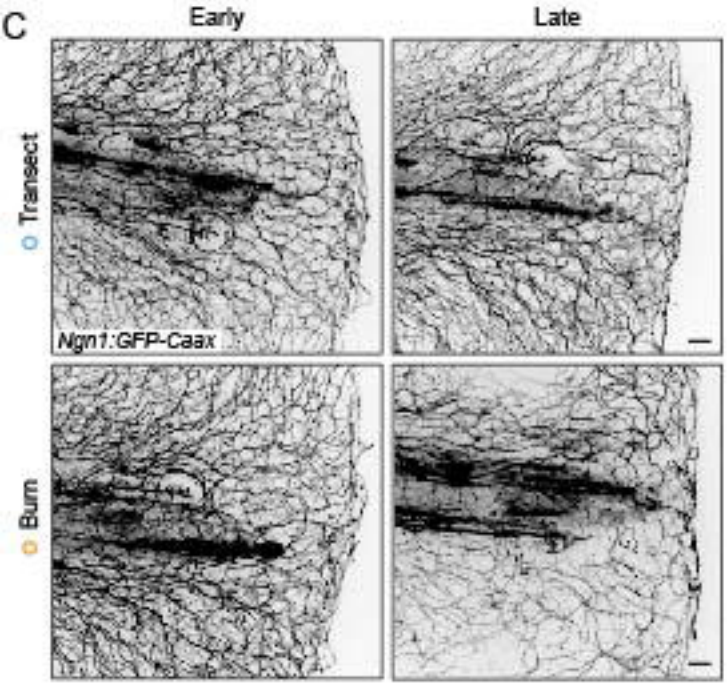
Early
Late
Transect
Burn
Ngn1:GFP-Caax

D

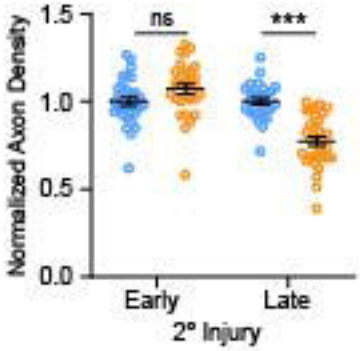
Normalized Axon Density
1.5
1.0
0.5
0.0
ns
***
Early
Late
2° Injury

E

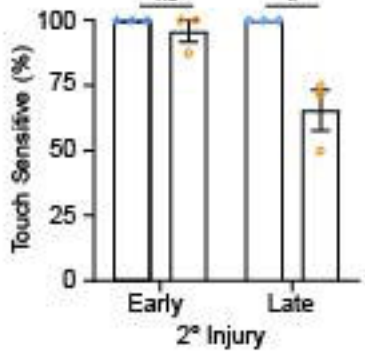
Touch Sensitive (%)
100
75
50
25
0
ns
*
Early
Late
2° Injury

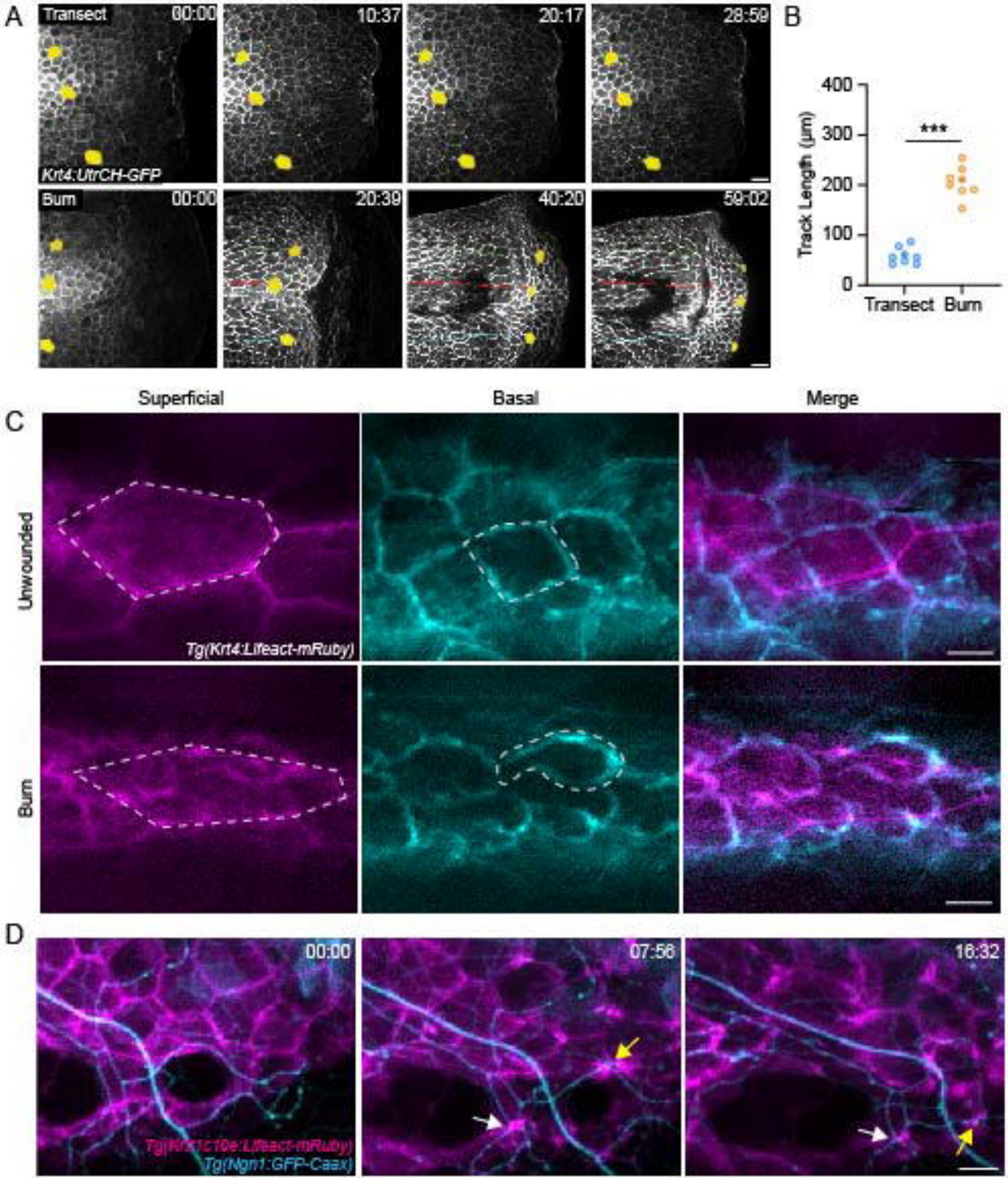
A
Transect
00:00
10:37
20:17
28:59
Krt4:UtrCH-GFP
Burn
00:00
20:39
40:20
59:02
B
Track Length (µm)
400
300
200
100
0
***
Transect
Burn
C
Superficial
Basal
Merge
Unwounded
Burn
Tg(Krt4:Lifeact-mRuby)
D
00:00
07:56
16:32
Tg(Krt1c10e:Lifeact-mRuby)
Tg(Ngn1:GFP-Caax)

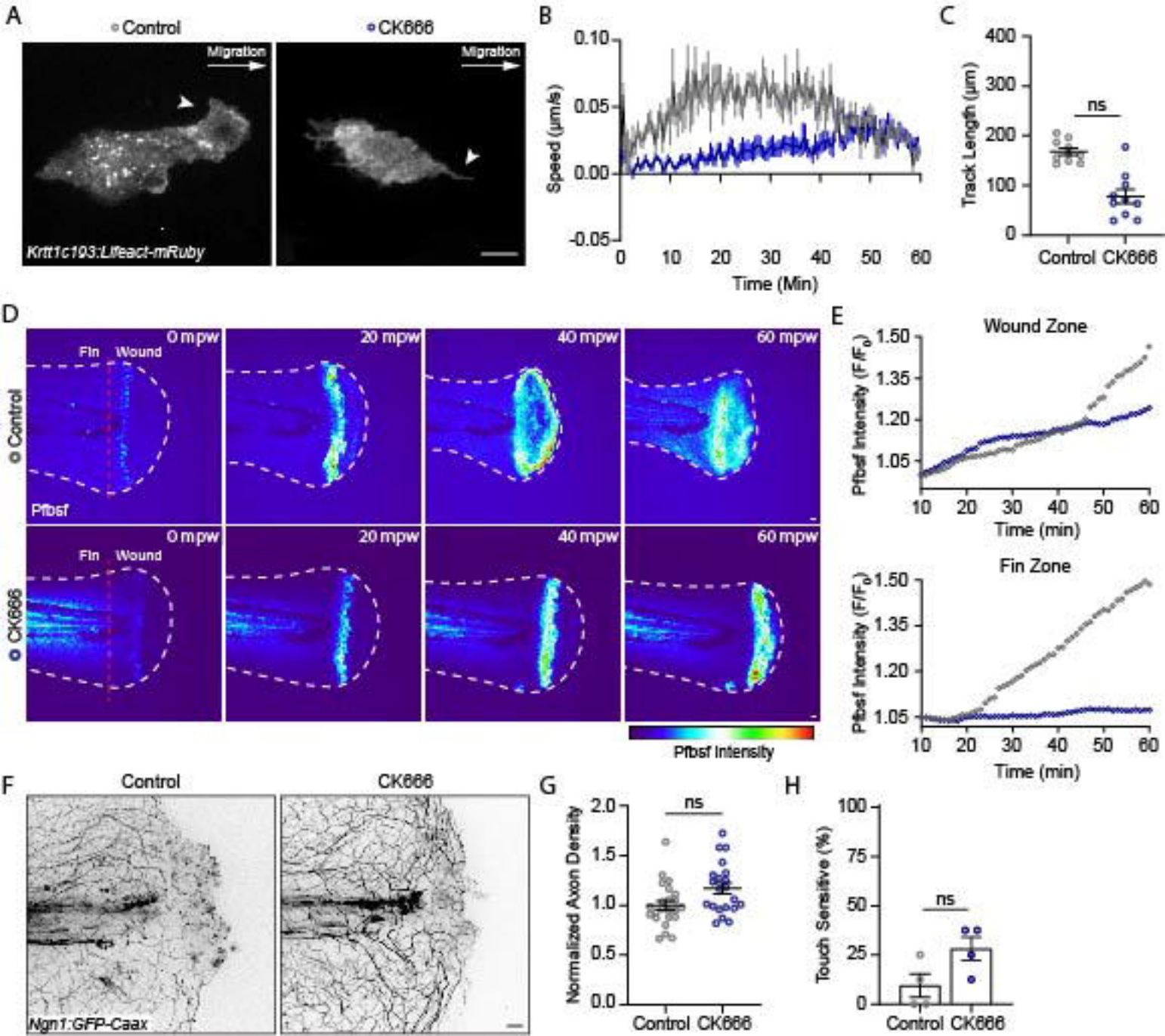
A
Control
CK666
Migration
Migration
Krtt1c1b3:Lifeact-mRuby
B
Speed (µm/s)
Time (Min)
C
Track Length (µm)
ns
Control
CK666
D
0 mpw
20 mpw
40 mpw
60 mpw
Fin
Wound
Control
CK666
Pfbsf
Pfbsf Intensity
E
Wound Zone
Fin Zone
Pfbsf Intensity (F/F0)
Time (min)
F
Control
CK666
Ngn1:GFP-Caax
G
Normalized Axon Density
ns
Control
CK666
H
Touch Sensitive (%)
ns
Control
CK666

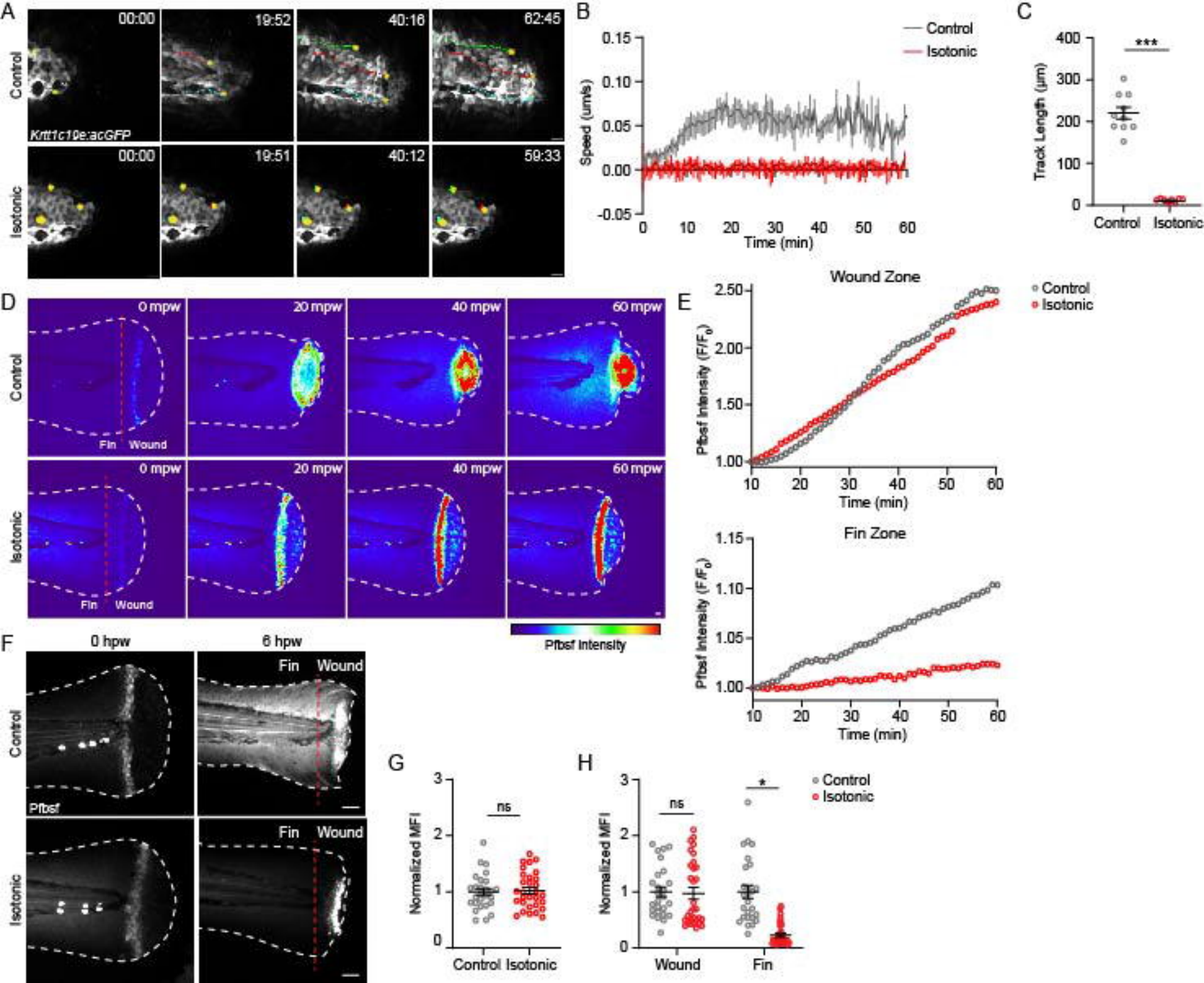
A
00:00
19:52
40:16
62:45
Control
Krtt1c19e:acGFP
00:00
19:51
40:12
59:33
Isotonic
B
Control
Isotonic
Speed (um/s)
Time (min)
C
Track Length (µm)
***
Control
Isotonic
D
0 mpw
20 mpw
40 mpw
60 mpw
Control
Isotonic
Fin
Wound
Pfbsf Intensity
E
Wound Zone
Fin Zone
Pfbsf Intensity (F/F0)
Time (min)
Control
Isotonic
F
0 hpw
6 hpw
Fin
Wound
Pfbsf
G
Normalized MFI
ns
Control
Isotonic
H
Normalized MFI
ns
*
Wound
Fin
Control
Isotonic

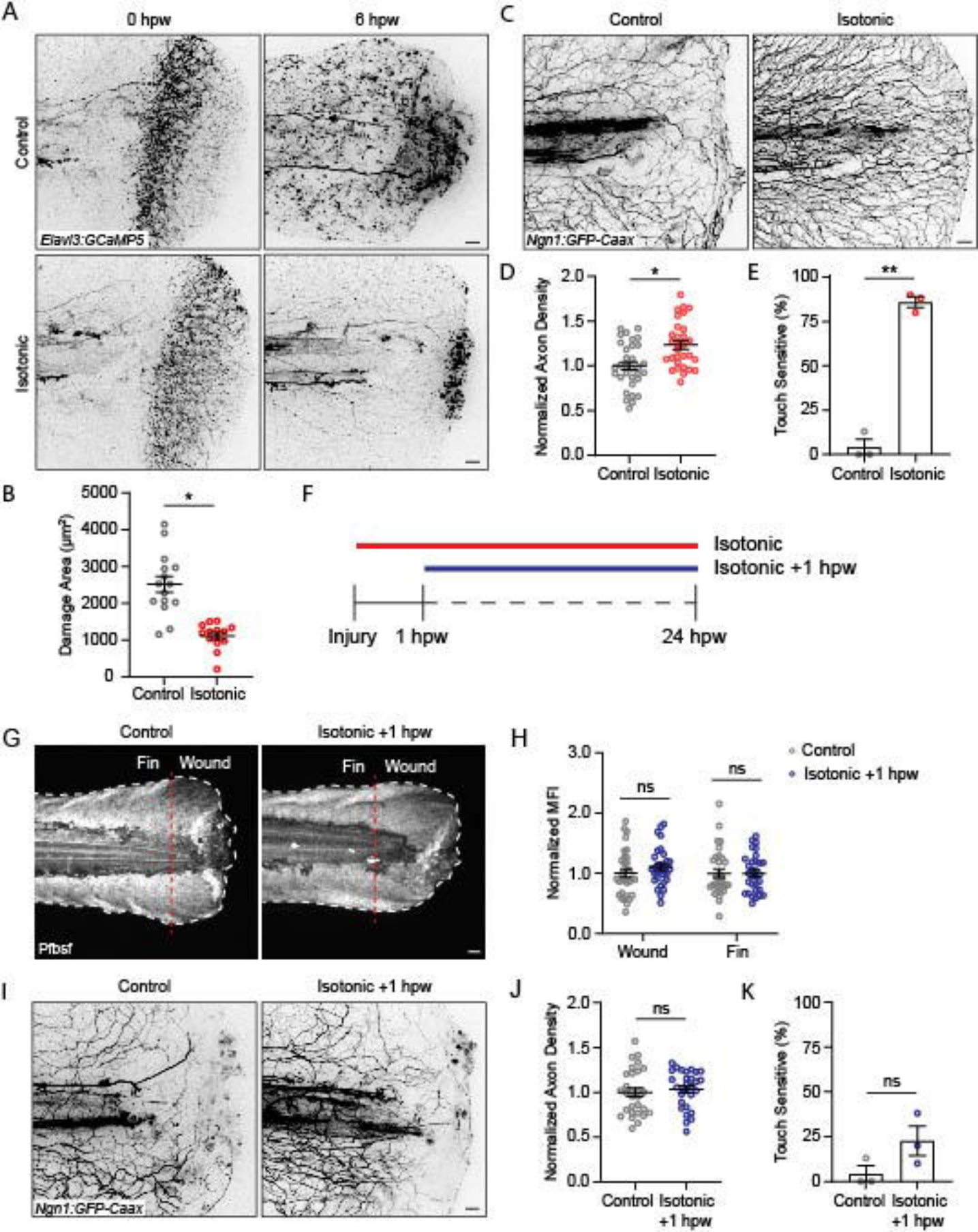
A
0 hpw
6 hpw
Control
Isotonic
Elavl3:GCaMP5
C
Control
Isotonic
Ngn1:GFP-Caax
D
Normalized Axon Density
Control Isotonic
E
Touch Sensitive (%)
Control Isotonic
B
Damage Area (μm²)
Control Isotonic
F
Isotonic
Isotonic +1 hpw
Injury 1 hpw 24 hpw
G
Control
Isotonic +1 hpw
Fin Wound
Pfbsf
H
Normalized MFI
Control
Isotonic +1 hpw
ns
Wound Fin
I
Control
Isotonic +1 hpw
Ngn1:GFP-Caax
J
Normalized Axon Density
Control Isotonic +1 hpw
K
Touch Sensitive (%)
Control Isotonic +1 hpw